Bound states in the continuum in asymmetric crossbar junctions in one-dimensional waveguides

Sofia Pinto [,1] Rafael A. Molina [,2] and Pedro A. Orellana [1]

[1]*Departamento de Física, Universidad Técnica Federico Santa María, Casilla 110 V, 2340000 Valparaíso, Chile*
[2]*Instituto de Estructura de la Materia, CSIC, Serrano 123, E-28006 Madrid, Spain*

Over the past few decades, the study of bound states in the continuum (BICs), their formation, and properties has attracted a lot of attention, especially in optics and photonics. It is particularly noticeable that most of these investigations are based on symmetric systems. In this article, we study the formation of bound states in the continuum in electronic and photonic transport systems consisting of crossbar junctions formed by one-dimensional waveguides, considering asymmetric junctions with commensurable lengths for the upper and lower arms. These BICs in an asymmetric system go beyond the symmetry-protected paradigm. We also study how BICs form in linear junction arrays as a function of the distance between consecutive junctions and their commensurability with the upper and lower arms. New commensurability conditions in the array's central section also give rise to Fabry-Pérot-type BICs. We solve the Helmholtz equation for the crossbar junctions and calculate the transmission probability, local density of states in the intersections, and quality factor. The presence of quasi-BICs is reflected in the transmission probability as a sharp resonance in the middle of a symmetric Fano resonance, along with Dirac δ-functions in the probability density and divergence in the quality factors.

I. INTRODUCTION

Bound states in the continuum (BICs) are states that remain spatially localized and show no decay despite coexisting with the continuum of the radiation spectrum of the system [1,2]. Von Neumann and Wigner [3] first predicted them for quantum mechanics. In their work, they found a solution to the Schrödinger equation with a particular oscillating potential in which a bound state with discrete and positive energy coupled to the radiation continuum was formed due to multiple interference processes, resulting in the complete suppression of particle escape. For many decades, von Neumann and Wigner's results were considered nothing but a mathematical curiosity, probably due to the artificial characteristics of the potential they used to demonstrate the properties of BICs. In the 1970s and subsequent years, various theoretical studies presented energy states with the characteristics already mentioned, but the authors of those works did not relate the results obtained to the phenomenon of BICs [4]. Then, in 1985, Friedrich and Wintgen reformulated von Neumann and Wigner's concept of the BIC in a more general framework as a result of complete destructive interference of two resonances undergoing an avoided crossing [5]. More recent works showed that BICs could be made robust through symmetry arguments [6,7]. In this case, the coupling to the continuum is forbidden due to the conservation of some symmetry. BICs were then divided into two categories: the accidental ones, like in the works by Friedrich and Wintgen, and the symmetry-protected ones [1]. A new category of BICs can be related to large degeneracies induced by general lattice symmetries [8–10]. An important development was the realization that, on many occasions, a small symmetry breaking in the case of symmetry-protected BICs or a small change in parameters in the case of accidental BICs induces the appearance of Fano-like resonances that were later called quasi-BICs [11–13].

BICs, although first theoretically predicted in quantum mechanics, are a general wave phenomenon, which is reflected in the experimental situation. The first reported evidence of the formation of these states was made in an electronic system, a semiconductor heterostructure [14]. However, it was not until 2008 that symmetry-protected BICs were measured for the first time in an optical waveguide array [15]. In the past decade, the investigation of BICs has become an active topic, with experiments in photonics, phononics, plasmonics, and others, mainly due to their device-manufacturing applications [16]. With this increase of attention came an increase in the number of studies on different systems that may hold these exotic states [17–19], most of which based their research on symmetric properties. Accidental BICs have also been measured [13,20] and may have important applications as high-Q narrow-frequency resonators [21]. Other applications of BICs include sensors [22–24], lasers [25,26], filters [27], transducers [28], and actuators [29].

In this work, we study the appearance of BICs in asymmetric crossbar structures. The studied system corresponds to a quantum graph. These graphs are network systems composed of vertices connected at the edges, where a differential equation is defined at each edge [30,31]. Quantum graphs are meant to be effective models of multiply connected quasi-one-dimensional systems at low energies and have been widely investigated [31–33], mainly due to the simplicity of the models, allowing the understanding of complex physical phenomena. In particular, these models have been extensively used to study BICs, their properties, and formation mechanisms. Our analysis relies on a simple scattering

formalism of single-channel waveguides, which allows us to find analytical solutions and a deep understanding of the BIC formation mechanisms. The signatures of BICs in the transmission show sharp resonances in the middle of antiresonances when the commensurability between the lengths of the side-attached structures breaks slightly (they are called quasi-BICs in the literature [34–36]). The main result of our work is that, when the sidearms of the junction have commensurable dimensions, we find an alternative type of BIC that goes beyond the symmetry-protected BIC paradigm. We also extend our analysis to two or more crossbar structures in a series. The asymmetric BICs are still present and can even form bands for many scattering units. However, other BICs form due to the hybridization of the wave functions in the side-attached bars and the central channel. These extra BICs can be described by the previously known Fabry-Pérot mechanism for BIC formation. Finally, we discuss the possibility of using our setup as a sensor for the impurities or imperfections of the systems.

II. MODELS AND RESULTS

A. Single crossbar junction

First, we study the simplest setup, a system consisting of a single crossbar junction of single channel waveguides as shown in Fig. 1. The incident waves approach from the left and can be transmitted or reflected at the junction. The upper and lower arms are finite, with lengths L^+ and L^-, respectively. Note that this setup can be considered a varia-

tion of a Michelson-Morley interferometer [37]. However, the differences are important and allow bound states in vertical arms. Under particular circumstances, some of these bound states can decouple from the continuum in the horizontal waveguide. When these BICs form, there are clear signatures in the transmission spectrum, which we analyze below.

In Appendix A, we explain the analytical calculations for the scattering problem in this system. The final result for the total transmission probability is

$$T = |t|^2 = \frac{4}{4 + [\cot(kL^+) + \cot(kL^-)]^2}. \quad (1)$$

To understand the result, we apply the following variable changes:

$$L^+ = \left[n + \frac{\Delta}{2}\right]L_0, \quad (2)$$

$$L^- = \left[m - \frac{\Delta}{2}\right]L_0. \quad (3)$$

The variables n and m are integers, L_0 is some measure with units of length, and Δ is a dimensionless commensurability parameter. By making these changes, it becomes easier to analyze the impact of having commensurate top and bottom sidearm lengths. We simplify the final expressions by renaming k/π as k', which will be expressed in units of L_0^{-1} or, equivalently, in units of $\frac{1}{L_0}$.

We then rewrite Eq. (1) using the new variables:

$$T = \frac{4\sin^2\left[\pi k' L_0\left(n + \frac{\Delta}{2}\right)\right]\sin^2\left[\pi k' L_0\left(m - \frac{\Delta}{2}\right)\right]}{4\sin^2\left[\pi k' L_0\left(n + \frac{\Delta}{2}\right)\right]\sin^2\left[\pi k' L_0\left(m - \frac{\Delta}{2}\right)\right] + \sin^2[\pi k' L_0(n + m)]}. \quad (4)$$

Analyzing the previous expression we see that, for $\Delta = 0$, there will be symmetric Fano resonances [38] for every value of k' that meets the following conditions:

$$k' = \frac{s}{n}\left(\text{units of } \frac{1}{L_0}\right) \quad \text{and/or}$$

$$k' = \frac{p}{m}\left(\text{units of } \frac{1}{L_0}\right) \quad \forall (s, p) \in \mathbb{N}. \quad (5)$$

In addition, the value of T will become undetermined for $\Delta = 0$ and every value of k' that meets the condition

$$\exists (s, p) \in \mathbb{N} \quad : k' = \frac{s}{n}\left(\text{units of } \frac{1}{L_0}\right) = \frac{p}{m}\left(\text{units of } \frac{1}{L_0}\right). \quad (6)$$

This mathematical condition of commensurable lengths marks the presence of a BIC in the system at these values of the renormalized momentum k'. As BICs do not couple to the continuum, they cannot be observed in the transmittance of the system. However, any small rupture of commensurability turns the BIC into a quasi-BIC, which appears as a narrow spectral resonance. So for $\Delta \to 0$ and the same commensu-

rability condition, we obtain $T = 1$. This is the signature of BICs in the transmission spectrum.

Figure 2 displays the transmission probability (top) and local density of states (bottom) for a single-crossbar junction, with $n = 2$ and $m = 3$, for two cases: commensurability between the upper and lower arms with $\Delta = 0$ (right) and rupture of this commensurability with $\Delta = 0.001$ (left). As predicted, we can appreciate the formation of Fano resonances in every value of k' that meets the condition stated in Eq. (5) and the appearance of quasi-BICs for the rupture of commensurability with $\Delta = 0.001$ for every value of k' that meets the condition stated in Eq. (6), which leads us to recognize the formation of BICs for these same values of k' for the case of absolute commensurability ($\Delta = 0$).

On the other hand, when computing the local density of states in the system, we notice the appearance of sharp peaks for the same values of k' at which quasi-BICs appear in the case of $\Delta = 0.001$. These peaks correspond to Dirac-δ with no width in the case of absolute commensurability ($\Delta = 0$), so they are represented by a dashed line. The appearance of these Dirac-δ confirms the formation of BICs for the values of k' already mentioned.

It is possible to interpret the interesting results and the commensurability condition by considering that the vertical
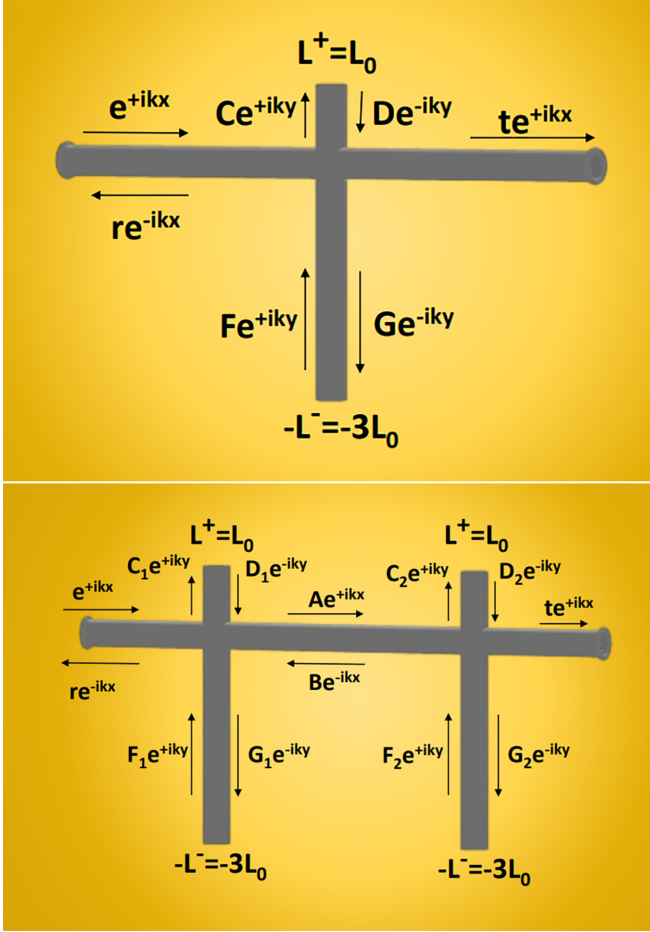
FIG. 1. Two setups consisting of a single crossbar junction in a one-dimensional waveguide (top) and a double crossbar junction (bottom). The system is open through its horizontal arms and remains closed at the ends of its vertical arms, with their respective lengths being L^+ (in the cases shown, L_0) and L^- (in the cases shown, $3L_0$).
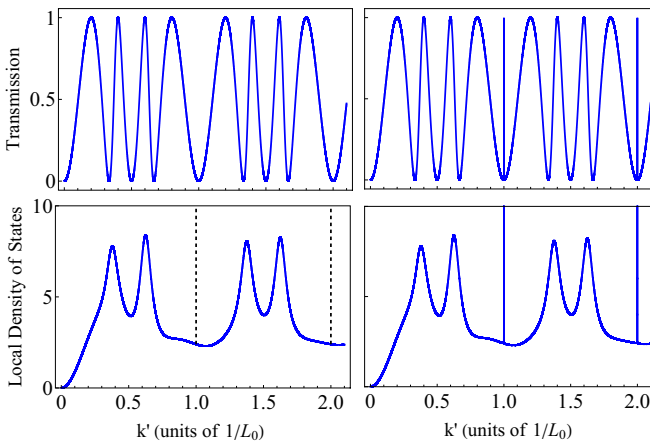

FIG. 2. Results for the transmission (top) and local density of states (bottom) vs k' for a single-crossbar junction with $n = 2$ and $m = 3$. The right panels show the results for full commensurability between the upper and lower arms ($\Delta = 0$), while the left panels consider a small breaking of the commensurability ($\Delta = 0.001$).
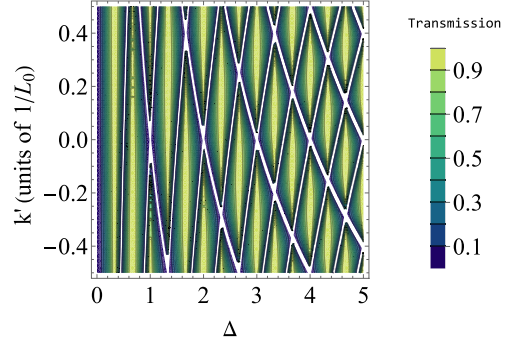

FIG. 3. Contour plot of the transmission as a function of parameters k' and Δ with $n = 1$ and $m = 2$.

top and bottom arms form an infinite well. The states in the well are not affected by the continuum if there is a node of their wave function in the connection to the transmission waveguides. More information can be found in Appendix B.

Figure 3 displays a contour plot of the transmission as a function of the renormalized momenta k' and the asymmetry parameter Δ for the case $n = 1$ and $m = 2$. The plot clearly shows the evolution of the BICs into quasi-BICs and then into more standard resonances as Δ increases.

The discovered BICs do not fit into the categories described in previous works. Although they follow a formation mechanism similar to symmetry-protected BICs, the described system does not meet the necessary conditions to enter such a category, as it is clearly asymmetric. Therefore, these states belong to a different category of BIC formation, depending solely on the commensurability of their dimensions.

Now, we analyze the dependence of the quasi-BIC's width on the perturbation parameter Δ. In the case of single-channel waveguides, an elastic perturbation in the arms can change only the optical path and is equivalent to the Δ parameter defined earlier. For simplicity, we consider the case with $n = 1$ and $m = 2$ without loss of generality. First, let us assume the equation for the transmission, Eq. (4). In the limit $\Delta \ll 1$ and the vicinity of $k' = 1$(units of $\frac{1}{L_0}$), we can write the equation for the transmission, Eq. (4), as

$$T \approx \frac{4\sin^2(2\pi k' L_0)}{5 + 4\cos(2\pi k' L_0)} + \frac{4\sin^4\left(\frac{\pi\Delta}{2}\right)}{4\sin^4\left(\frac{\pi\Delta}{2}\right) + \sin^2(3k'\pi L_0)}. \quad (7)$$

We can then identify two different contributions to this equation. The first contribution goes to zero for $k' = \frac{f}{2}$(units of $\frac{1}{L_0}$), with f being an integer, and describes the interference effects and Fano resonances that appear for $\Delta = 0$. The second contribution has the form of a Breit-Wigner resonance $[T(x) = \Gamma^2/(\Gamma^2 + x^2)]$ with width $\Gamma = 2\sin^2(\pi\Delta/2)$ for $x = \sin(3\pi k' L_0)$. For small values of Δ and $x = k' L_0$ the width is just $\Gamma \approx (\frac{\Delta^2\pi}{6})$.

From the above equation, we can see that, for small perturbations $\Delta \ll 1$, the width of the quasi-BIC is proportional to the quadratic value of the perturbation parameter Δ^2. This formula should be helpful for the use of the system's BICs in metrological and sensing applications. In Fig. 4, we show a comparison of the exact result with the Breit-Wigner approximation for two values of the perturbation, $\Delta = 0.05$ and
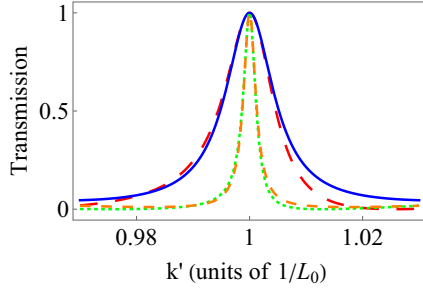
FIG. 4. Transmission vs k' for a single-crossbar junction with $n = 1$ and $m = 2$. The red long-dashed and green short-dashed lines show the exact results from Eq. (4) considering $\Delta = 0.05$ and $\Delta = 0.1$, respectively, while the blue solid and orange medium-dashed lines show the approximation given by Eq. (7). For these values of Δ, both curves overlap.

$\Delta = 0.1$, showing good agreement even for not very small values of Δ.

Using Eq. (7), we can gather the data needed to calculate the Q factor for this setup considering $n = 1$ and $m = 2$. The Q factor, in this case, is represented by $Q_1 = \pi/\Gamma$. The Q-factor graph is shown in Fig. 5, with the asymmetry parameter Δ being the independent variable. As we can see, this setup can achieve an ultrahigh Q factor that diverges at the resonances.

B. Array of N crossbar junctions

We now study a generalization of the previous system consisting of an array with N identical cross junctions equally spaced from one another. The separation length is given by the parameter a. As before, the system is open through its horizontal arms and remains closed at the ends of its vertical arms, with their respective lengths being L^+ (upper arm) and L^- (lower arm).

We use the transfer-matrix method [39] to find the transmission probability for this system, as explained in Ap-
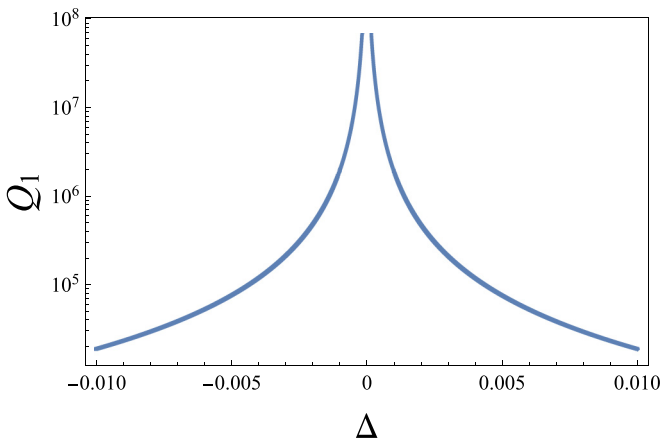

FIG. 5. Q factor as a function of the asymmetry parameter Δ for $N = 1$ considering $n = 1$ and $m = 2$.
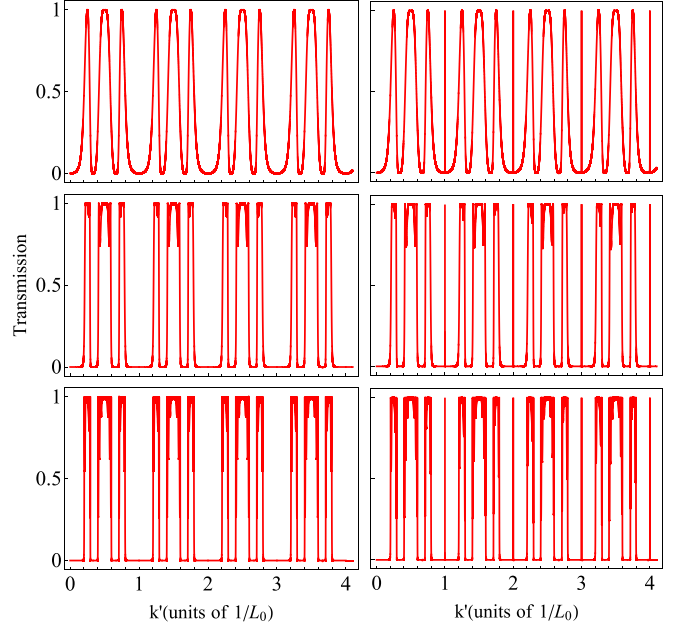

FIG. 6. Transmission vs k' for a system formed by different numbers of crossbar junctions for $n = 1$, $m = 3$, $l = 5$, and $\nu = 0$. From top to bottom, the three rows show the cases with $N = 2$, $N = 5$, and $N = 10$, respectively. The left panels show the results for $\Delta = 0$, and the right panels show the results for $\Delta = 0.01$.

pendix C. The final result is

$$T_N(k) = \frac{1}{1 + \left[\frac{|\alpha| \sin(Nql)}{2\sin(ql)}\right]^2}, \qquad (8)$$

with the parameter $\alpha = i[\cot(kL^+) + \cot(kL^-)]$ and

$$\cos(ql) = \cos(ka) - \frac{[\cot(kL^+) + \cot(kL^-)]\sin(ka)}{2}. \qquad (9)$$

To analyze the transmission through the junction array and the formation of BICs in the system, we make the variable changes in Eqs. (2) and (3), as well as the following change:

$$a = [l + \nu]L_0, \qquad (10)$$

where the new parameter l is also an integer. The parameter ν is a commensurability parameter that will play a similar role to Δ but for the central region.

Careful examination of Eq. (8) reveals that there is perfect transmission independent of the incident momentum for some highly symmetric cases. We do not explore these cases further in this work as we focus on BICs.

Figure 6 displays the transmission profiles for an N-junction system with different values of N. From top to bottom, we show $N = 2$, $N = 5$, and $N = 10$. We set $n = 1$, $m = 3$, $l = 5$, and $\nu = 0$ for all cases. We compare the cases with $\Delta = 0$ (left panels) with those with $\Delta = 0.01$ (right panels). We observe the progressive formation of a band structure as the value of N is increased. This band structure replaces the pattern shown in the transmission of resonances and antiresonances in the single cross junction. When $\Delta \neq 0$, new narrow bands from the quasi-BICs appear in the middle of the forbidden region with almost zero transmission.
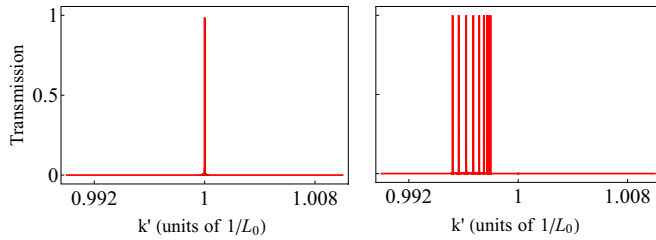
FIG. 7. Zoom of the first quasi-BIC structure formed for $N = 10$ crossbar junctions with $n = 1$, $m = 3$, and $l = 5$. The left panel shows $\Delta = 0.01$ and $\nu = 0$, while the right panel shows $\Delta = 0$ and $\nu = 0.01$.

Figure 7 shows zooms of the band structures formed for $N = 10$ crossbar junctions with $n = 1$, $m = 3$, and $l = 5$ around $k' = 1$ (units of $\frac{1}{L_0}$), where the formation of the first quasi-BICs occurs. From the images, it is apparent that the quasibound states in the continuum (quasi-BICs) which were initially thought to be single sharp resonances can be a series of peaks that are extremely close to each other, as in the case shown in the right panel. Eventually, as commensurability becomes full, these quasi-BICs merge into a single BIC. Increasing the number of cross junctions in the system leads to a rise in maxima formed when commensurability is broken. With proper calibration and depending on the spectral resolution of the detectors, these crossbar junction arrays could be employed to enhance sensitivity for BIC applications in sensing and metrology.

BICs occur when the lengths from the upper and lower arms of the system are commensurable, as previously mentioned. Additionally, BICs will also appear when one of the arms is commensurable with the new separation length between consecutive intersections. Generally, based on Eq. (C21), BICs will be formed for every value of k' that satisfies the following condition:

$$\exists \{j_1, j_2\} \subset \{n, m, l\} \wedge \exists \{s, p\} \in \mathbb{N} :$$

$$k' = \frac{s}{j_1}\left(\text{units of } \frac{1}{L_0}\right) = \frac{p}{j_2}\left(\text{units of } \frac{1}{L_0}\right). \quad (11)$$

Thus, if any two of these three lengths (n, m, and l) are commensurate, there will be a BIC at such a value of k'. Considering this condition and the discussion in Appendix B, it is evident that the well states that give rise to BICs due to their nodal structure can be the same as before or can be hybridized states between the central region and either the top or the bottom sidearm. The commensurate condition with a implies that the stationary states formed by this hybridization have nodes at $x = (j - 1)a$ and $x = ja$ in addition to canceling at $y = L^+$ or $y = L^-$. These hybridized states are the continuum equivalent of compact localized states in lattice models [40]. Similarly, like these compact localized states do in infinite systems, they form BIC flat bands that become quasi-BIC very narrow bands under infinitesimal perturbations.
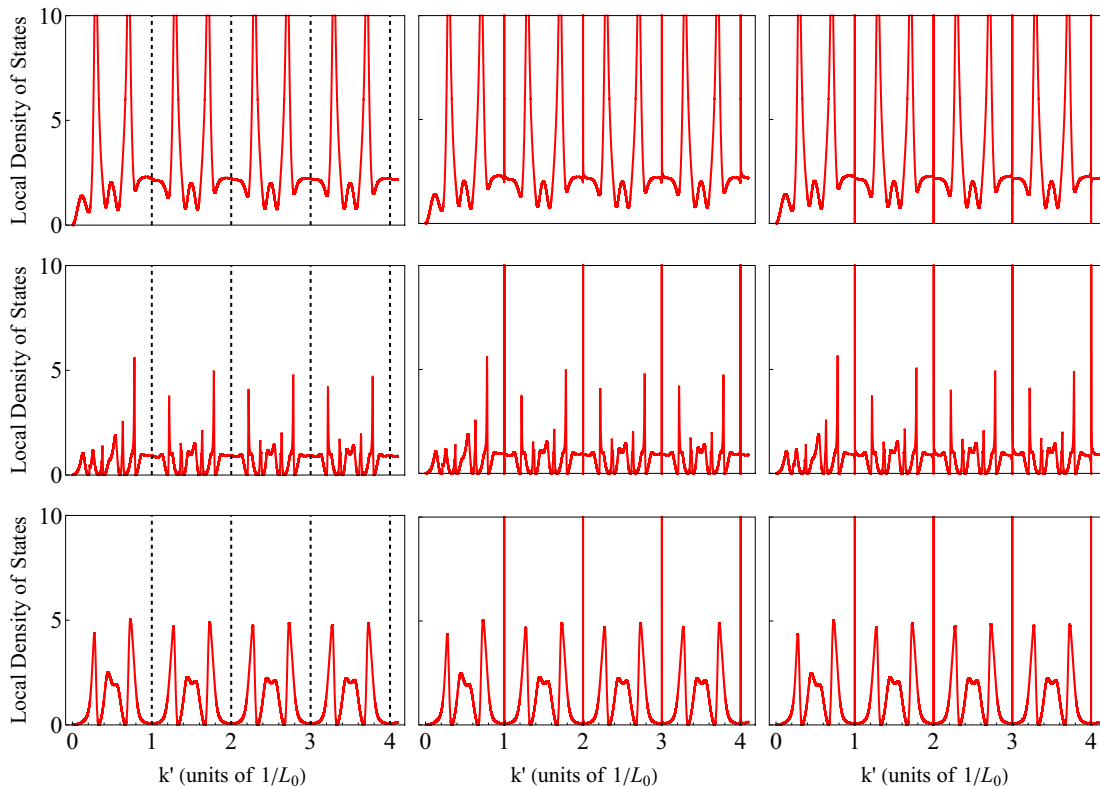

FIG. 8. Local density of states vs k' for a system formed by $N = 2$ crossbar junctions for $n = 1$, $m = 3$, and $l = 5$. From top to bottom, the three rows show the local density of states for the arms of the first crossbar (entrance), middle section, and the arms of the second crossbar (exit), respectively. The left panels show the results for $\Delta = \nu = 0$, the middle panels show the results for $\Delta = 0.001$ and $\nu = 0$, and the right panels show the results for $\Delta = 0$ and $\nu = 0.001$.
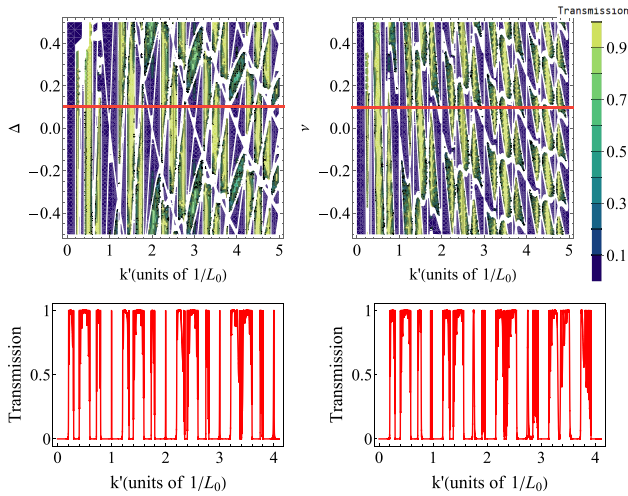
FIG. 9. Top panels show contour plots for the transmission with $n = 1$, $m = 3$, $l = 5$, and $N = 10$ as a function of Δ and k', with $\nu = 0$ (left) and ν and k' with $\Delta = 0$ (right). Red lines mark specific sections of these contour plots shown in the bottom panels with the corresponding transmission plots as a function of k' with $\Delta = 0.1$ and $\nu = 0$ (left) and $\Delta = 0$ and $\nu = 0.1$ (right).

Figure 8 displays the local density of states for the system with $N = 2$, $n = 1$, $m = 3$, and $l = 5$ (see Appendix D for the analytical calculations). From top to bottom, the three rows show the local density of states for the arms of the first crossbar (entrance), the middle section, and the arms of the second crossbar (exit), respectively. The left panels show the results for $\Delta = \nu = 0$, the middle panels show the results for $\Delta = 0.001$ and $\nu = 0$, and the right panels show the results for $\Delta = 0$ and $\nu = 0.001$. Once again, the appearance of Dirac δ-functions (with no width for the case of full commensurability) for the same values of k' at which they appear as sharp resonances in the transmission profile confirms the formation of BICs for the values of k' already mentioned.

Based on the literature [1,2], BICs are formed by several mechanisms, such as the symmetry-protected and Fabry-Pérot mechanisms. The latter occurs when two separated resonators have a perfect reflection. As we already showed in our analysis of the single-crossbar-junction system, we can extend the symmetry-protection mechanism to nonsymmetric systems with commensurable dimensions. In the case of the system formed by an array of N identical equally spaced crossbar junctions, not all of the observed BICs are attributable to this mechanism. Since some BICs appear depending on the length of the region between crosses, we can attribute their formation to the Fabry-Pérot mechanism. This structure is similar to the one analyzed in Ref. [41].

Figure 9 shows a contour plot of the transmission for a system with $N = 10$, $n = 1$, $m = 3$, and $l = 5$. In the left panels, we show the case with $\nu = 0$ as a function of Δ and k', while in the right panels, we show the case with $\Delta = 0$ as a function of ν and k'. The parameter Δ is symmetric between positive and negative values as the change in sign only switches the role of the upper and lower arms of the junction. However, the parameter ν shows clear asymmetry between positive and negative values because larger or smaller
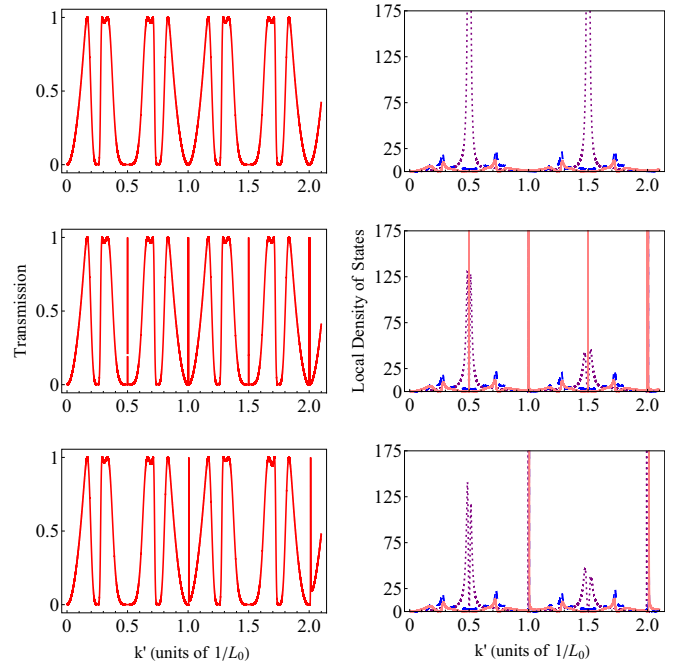

FIG. 10. System formed by $N = 2$ crossbar junctions with measures $n = 4$, $m = 2$, and $l = 1$. The left panels correspond to the transmission, while the right panels show the local density of states for different regions separated by colors: blue (large dashed) lines for the arms in the first crossbar, purple (small dashed) for the middle section, and pink (continuous) lines for the arms in the second crossbar. From top to bottom, the three presented rows correspond to $\Delta = \nu = 0$, $\Delta = 0.01$ with $\nu = 0$, and finally $\nu = 0.01$ with $\Delta = 0$.

central regions change the commensurability conditions of the arms differently.

Figure 10 displays the transmission and local density of states of a system consisting of two crossbar junctions with dimensions of $n = 4$, $m = 2$, and $l = 1$. In the right panels, the colored curves represent the local density of states for three different regions: the arms of the first crossbar, the middle region, and the arms of the second crossbar. According to expression (11), we expect BICs to form for values of $k' = \frac{s}{2}$ (units of $\frac{1}{L_0}$), with s being an integer. Considering the formation of quasi-BICs shown in the middle and bottom panels (where the system's commensurability has been broken with $\Delta = 0.01$ and $\nu = 0.01$, respectively), we confirm the formation of BICs for the expected values. Depending on the breaking that we have in the system's commensurability, different quasi-BICs form. In the middle panels the rupture occurs between n and m, between n and l, and between m and l, so quasi-BICs are formed for every value of $k' = \frac{s}{2}$ (units of $\frac{1}{L_0}$). These quasi-BICs appear in the profiles of the local density of states as a superposition of very narrow peaks for the different regions of the system. In this case, quasi-BICs are formed in the arms of both crossbar junctions but not in the middle section; this is a superposition of the blue long-dashed and pink solid almost Dirac-δ lines in the profile. On the other hand, in the bottom panels, the rupture occurs only between n and l and m and l. However, commensurability between n and m remains unbroken. That is why quasi-BICs form for only integer values of k' as $k' = \frac{s}{1}$ (units of $\frac{1}{L_0}$), with $s \in \mathbb{N}$. In this

case, quasi-BICs are formed in both crossbar junctions and in the middle section; this is a superposition of the blue long-dashed, pink solid, and purple short-dashed narrow peaks in the profile.

III. T-SHAPED JUNCTIONS

A T-shaped junction is a particular case of our crossbar junction model with one of the lengths going to zero. For example, let us set $L^- = 0$; the transmission formula is then simplified to

$$T = |t|^2 = \frac{4}{4 + [\cot(kL^+)]^2}. \tag{12}$$

All allowed momenta in the infinite well of length L^+ become BICs and, with the condition for BIC formation, become $k_j = j\frac{\pi}{L^+}$. A change in the length of the sidearm does not induce a quasi-BIC but moves the position of the BIC in the momenta. Recently, BICs in this kind of structure were explored experimentally for radio-frequency circuits [42].

In the case of a T-shaped junction array, we recover a commensurability condition between the length of the sidearm L^+ and the central region between two consecutive junctions a. The results can also be obtained as the limit for the crossbar junction arrays with $L^- = 0$. The commensurability condition for the existence of BICs then becomes

$$\exists (s, p) \in \mathbb{N} \ :$$
$$k' = \frac{s}{n}\left(\text{units of } \frac{1}{L_0}\right) = \frac{p}{l}\left(\text{units of } \frac{1}{L_0}\right). \tag{13}$$

Then, the states of the system that give rise to BICs are hybridized states between the sidearm and the central region.

IV. SUMMARY AND CONCLUSIONS

In summary, we studied the formation of BICs in a system consisting of crossbar and T-shaped junctions in one-dimensional waveguides. To solve the problem, we used the transfer-matrix method. We calculated the transmission spectrum and the local density of states of the structure. First, we investigated a single-crossbar junction and found the formation of BICs, even in highly asymmetric structures, as long as the upper and lower arms of the crossbar junctions had commensurable lengths. The formation mechanism of these BICs, despite their similarities to the paradigm of symmetry-protected BICs, does not correspond to the formation mechanisms studied and described in previous works [1]. It constitutes an alternative way of categorizing these peculiar states: BICs formed in nonsymmetric systems that exhibit commensurability of their dimensions. Second, we showed another mechanism for forming BICs due to the hybridization of the states in the intercrossbar region or a T-shaped junction with the states of the arms of the junctions. In addition, we identified a third mechanism for forming BICs by indirectly coupling two junction levels through the common unidimensional channel. An important aspect of our work is that the simplicity of the studied models allows for complete analytical treatment and a good understanding of the mechanisms behind the formation of such elusive states as these BICs.

In conclusion, we characterized the formation of BICs in asymmetric systems, with the condition of commensurability between the different sections of the structure. Furthermore, another mechanism that contributes to the formation of BICs, which is connected to the Fabry-Pérot mechanism, was identified. This mechanism uses two consecutive crossbar structures as perfect mirrors, generating stationary waves within the effective cavity that decouples from the continuum. Our results could be applied to developing sensors because we have studied how the width and the Q factor of the quasi-BICs depend on a perturbation. Our results go beyond the symmetry-protected BIC paradigm and may inspire a new search for BICs and their applications in different wave systems. We expect the BICs reported in this work to be observed in many different classical and quantum wave systems. An interesting setup to observe these states would be standing waves in acoustic waveguides with resonant cavities based on the work carried out by Huan *et al.* [19]. A simple extension of the experimental setup by Khattou *et al.* with stubbed structures in coaxial cables working in the radio-frequency domain [42] should allow us to test our results. Moreover, our work raises questions to answer in future investigations and the possibility of interesting extensions. What would the role of disorder be in the case of junction arrays? What happens if we increase the dimensionality of the arrays? Can the results be extended to multichannel systems? The condition for BICs will probably depend on the mode, but this dependence may have interesting applications for mode selectivity. Engineering the lengths and couplings in our models, it should be possible to induce nontrivial topology in the arrays, as has already been done in different photonic systems [42,43]. It would be exciting to check whether the analytical results can be obtained for nontrivial topological systems. Studying the anomalous, highly symmetric cases mentioned earlier for the array of N identical cross junctions with perfect transmission would also be interesting. We plan to explore all these aspects in future works.

APPENDIX A: ANALYTIC SOLUTION OF THE SINGLE-CROSSBAR JUNCTION

In this Appendix, we present the analytic solution for the scattering problem of the single-crossbar junction as presented in Fig. 1.

We separate the system into four sections: the left arm is section 1, the right arm is section 2, the upper part is section 3, and the lower part is section 4. Each of these sections has an associated wave function. We consider an incident wave plane from the left, reflecting with amplitude r and transmitting with

amplitude t:

$$\Psi_1(x) = e^{ikx} + re^{-ikx}, \tag{A1}$$

$$\Psi_2(x) = te^{ikx}, \tag{A2}$$

$$\Psi_3(y) = Ce^{iky} + De^{-iky}, \tag{A3}$$

$$\Psi_4(y) = Fe^{iky} + Ge^{-iky}. \tag{A4}$$

We seek to determine the amplitudes r, t, C, D, F, and G, for which we must apply the corresponding boundary conditions [44]. The wave function must be continuous at every point, so considering the junction point $x = y = 0$, the first condition to be fulfilled is

$$\Psi_1(0) = \Psi_2(0) = \Psi_3(0) = \Psi_4(0)$$
$$\implies t = 1 + r = F + G = C + D. \tag{A5}$$

Second, we assume that wave functions at the ends of both vertical arms (sections 3 and 4) go to zero, which mathematically implies

$$\Psi_3(L^+) = 0 \implies D = -Ce^{2ikL^+}, \tag{A6}$$

$$\Psi_4(-L^-) = 0 \implies F = -Ge^{2ikL^-}. \tag{A7}$$

The last condition states that the difference between the derivatives of the wave functions in the horizontal direction and those of the vertical direction must take the same value at the intersection point:

$$\left.\frac{\partial \Psi_2}{\partial x}\right|_{0^+} - \left.\frac{\partial \Psi_1}{\partial x}\right|_{0^-} = \left.\frac{\partial \Psi_3}{\partial y}\right|_{0^+} - \left.\frac{\partial \Psi_4}{\partial y}\right|_{0^-}. \tag{A8}$$

These conditions impose the following relation among the wave-function coefficients in the different regions:

$$t + r - 1 = C + G - D - F. \tag{A9}$$

We must solve for coefficients r (reflection amplitude), t (transmission amplitude), C, D, F, and G using Eqs. (A5) to (A9). The explicit solution can be written as follows:

$$t = \frac{2}{2 - i[\cot(kL^+) + \cot(kL^-)]}, \tag{A10}$$

$$r = \frac{2}{2 - i[\cot(kL^+) + \cot(kL^-)]} - 1, \tag{A11}$$

$$F = \frac{2e^{ikL^-}}{4i\sin(kL^-) + 2\sin(kL^-)[\cot(kL^+) + \cot(kL^-)]}, \tag{A12}$$

$$G = \frac{-2e^{-ikL^-}}{4i\sin(kL^-) + 2\sin(kL^-)[\cot(kL^+) + \cot(kL^-)]}, \tag{A13}$$

$$C = \frac{-2e^{-ikL^+}}{4i\sin(kL^+) + 2\sin(kL^+)[\cot(kL^+) + \cot(kL^-)]}, \tag{A14}$$

$$D = \frac{2e^{ikL^+}}{4i\sin(kL^+) + 2\sin(kL^+)[\cot(kL^+) + \cot(kL^-)]}. \tag{A15}$$

From the squared transmission amplitude $|t|^2$ we can compute the total transmission as in Eq. (1) in the main text.

We can also find the local densities of states as a function of k for the upper and lower sections of the crossbar junction,

which are respectively given by

$$P_3 = \int_{y=0}^{y=L^+} |\Psi_3|^2 dy$$
$$= \frac{-2\cot(kL^+) + 2kL^+\csc(kL^+)^2}{k\{4 + [\cot(kL^+) + \cot(kL^-)]^2\}}, \tag{A16}$$

$$P_4 = \int_{y=-L^-}^{y=0} |\Psi_4|^2 dy$$
$$= \frac{-2\cot(kL^-) + 2kL^-\csc(kL^-)^2}{k\{4 + [\cot(kL^+) + \cot(kL^-)]^2\}}. \tag{A17}$$

APPENDIX B: QUANTUM WELL SOLUTION

We can apply the solution of a well with infinite walls to the vertical sidearms. Taking the textbook solution for the infinite-potential well [44], the allowed momenta of the stationary waves solving the problem are then

$$k_j = j\frac{\pi}{L^+ + L^-}, \tag{B1}$$

with $j \in \mathbb{N}$. The corresponding wave functions

$$\Psi_j = A\sin\left[k_j\left(y - y_c + \frac{L^+ + L^-}{2}\right)\right], \tag{B2}$$

where A is the normalization constant and $y_c = (L^+ - L^-)/2$ is the middle point of the well. It is easy to get the condition for the wave function to have a node at the connection point with the transmission lines $\Psi_j(0) = 0$ when $L^+ = nL_0$ and $L^- = mL_0$, with $\Delta = 0$ as in the definitions of Eqs. (2) and (3):

$$k = s\pi\left(\text{units of } \frac{1}{L_0}\right), \tag{B3}$$

with $s \in \mathbb{N}$, which, when taking into account the allowed momenta (B1), is equivalent to the condition written in Eq. (6) in the main text.

APPENDIX C: ANALYTIC SOLUTION OF THE ARRAY OF N IDENTICAL CROSSBAR JUNCTIONS

In this Appendix, we present in detail the analytic solution for the scattering problem of the array of N crossbar junctions presented in Sec. II B and solved through the transfer-matrix method. The transfer matrix is the matrix that connects the waves to the right of the system with the waves to the left of the system as opposed to the scattering matrix that connects outgoing waves to incoming waves [39].

First, let us consider the jth cross junction from the array, placed in the position $x = (j - 1)a$, as shown in Fig. 11.

Like we did for the single-junction case, we separate the system into four sections: the left arm is described by the wave function $\Psi_{j-1}(x)$, the right arm is described by $\Psi_j(x)$, the upper arm is described by $\Phi_j^u(y)$, and the lower arm is described by $\Phi_j^d(y)$. In the end, considering plane-wave solutions, we
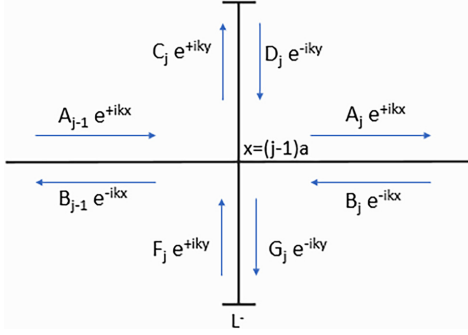
FIG. 11. jth cross junction from an array formed by N identical cross junctions equally spaced from one another. The studied junction is in position $x = (j-1)a$.

have

$$\Psi_{j-1}(x) = A_{j-1}e^{ikx} + B_{j-1}e^{-ikx}, \tag{C1}$$

$$\Psi_j(x) = A_j e^{ikx} + B_j e^{-ikx}, \tag{C2}$$

$$\Phi_j^u(y) = C_j e^{iky} + D_j e^{-iky}, \tag{C3}$$

$$\Phi_j^d(y) = F_j e^{iky} + G_j e^{-iky}. \tag{C4}$$

We now apply the corresponding boundary conditions, which are analogous to the ones described by Eqs. (A5) to (A8):

$$
\begin{aligned}
A_{j-1}e^{ik(j-1)a} &+ B_{j-1}e^{-ik(j-1)a} \\
&= A_j e^{ik(j-1)a} + B_j e^{-ik(j-1)a} \\
&= F_j + G_j = C_j + D_j,
\end{aligned} \tag{C5}
$$

$$\Phi_j^u(L^+) = 0 \implies D_j = -C_j e^{2ikL^+}, \tag{C6}$$

$$\Phi_j^d(-L^-) = 0 \implies F_j = -G_j e^{2ikL^-}, \tag{C7}$$

$$
\begin{aligned}
A_j e^{ik(j-1)a} &- B_j e^{-ik(j-1)a} - A_{j-1}e^{ik(j-1)a} \\
&+ B_{j-1}e^{-ik(j-1)a} \\
&= C_j - D_j - F_j + G_j.
\end{aligned} \tag{C8}
$$

Let us consider, for simplicity, the following variable changes in which we have absorbed the exponential into the coefficients:

$$A_j e^{ikja} = A_j' \quad \forall j, \tag{C9}$$

$$B_j e^{-ikja} = B_j' \quad \forall j. \tag{C10}$$

We can now write the equation system described by Eqs. (C5) to (C8) in its matrix form as

$$
\begin{pmatrix} A_j' \\ B_j' \end{pmatrix} = \begin{pmatrix} \left(1 + \frac{\alpha}{2}\right)e^{ika} & \frac{\alpha}{2}e^{ika} \\ -\frac{\alpha}{2}e^{-ika} & \left(1 - \frac{\alpha}{2}\right)e^{-ika} \end{pmatrix} \begin{pmatrix} A_{j-1}' \\ B_{j-1}' \end{pmatrix}. \tag{C11}
$$

For simplicity, we introduce a new parameter α, which corresponds to

$$\alpha = \frac{1 + e^{2ikL^+}}{1 - e^{2ikL^+}} + \frac{1 + e^{2ikL^-}}{1 - e^{2ikL^-}} = i[\cot(kL^+) + \cot(kL^-)]. \tag{C12}$$

With this, we find the transfer matrix that represents a single cross junction of the whole system:

$$\mathbf{M}_1 = \begin{pmatrix} \left(1 + \frac{\alpha}{2}\right)e^{ika} & \frac{\alpha}{2}e^{ika} \\ -\frac{\alpha}{2}e^{-ika} & \left(1 - \frac{\alpha}{2}\right)e^{-ika} \end{pmatrix}. \tag{C13}$$

The final transfer matrix for the whole array is given by the Nth power of the $\mathbf{M}_1$ matrix, that is,

$$\mathbf{M} = \mathbf{M}_1^N = \begin{pmatrix} \left(1 + \frac{\alpha}{2}\right)e^{ika} & \frac{\alpha}{2}e^{ika} \\ -\frac{\alpha}{2}e^{-ika} & \left(1 - \frac{\alpha}{2}\right)e^{-ika} \end{pmatrix}^N. \tag{C14}$$

From the latter expression, we notice $\det \mathbf{M}_1 = 1$, and we can use Chebishev's identity to compute the Nth power of the matrix.

Chebishev's identity states that for a matrix of the form

$$\mathbf{M} = \begin{pmatrix} a & b \\ c & d \end{pmatrix}, \tag{C15}$$

whose eigenvalues have the form

$$\lambda_1 = e^{iql}, \tag{C16}$$

$$\lambda_2 = e^{-iql}, \tag{C17}$$

its Nth power is given by

$$\mathbf{M}^N = \begin{pmatrix} a & b \\ c & d \end{pmatrix}^N = \begin{pmatrix} aU_{N-1} - U_{N-2} & bU_{N-1} \\ cU_{N-1} & dU_{N-1} - U_{N-2} \end{pmatrix}, \tag{C18}$$

where U_N is defined as a function of q as

$$U_N = \frac{\sin(N+1)ql}{\sin ql}. \tag{C19}$$

We can now obtain the final expression for the transfer matrix of the complete array by applying Chebishev's identity:

$$\mathbf{M} = \begin{pmatrix} \left(1 + \frac{\alpha}{2}\right)e^{ika}U_{N-1} - U_{N-2} & \frac{\alpha}{2}e^{ika}U_{N-1} \\ -\frac{\alpha}{2}e^{-ika}U_{N-1} & \left(1 - \frac{\alpha}{2}\right)e^{-ika}U_{N-1} - U_{N-2} \end{pmatrix}. \tag{C20}$$

Last, we can derive the transmission probability of this system from Eq. (C20):

$$T = \frac{1}{1 + \left[\frac{|\alpha|\sin(Nql)}{2\sin(ql)}\right]^2}. \tag{C21}$$

APPENDIX D: LOCAL DENSITY OF STATES OF AN ARRAY OF TWO IDENTICAL CROSSBAR JUNCTIONS

When considering a system formed by $N = 2$ identical crossbar junctions, it is reduced to the one shown in Fig. 12. From Eq. (8) we express the transmission probability for
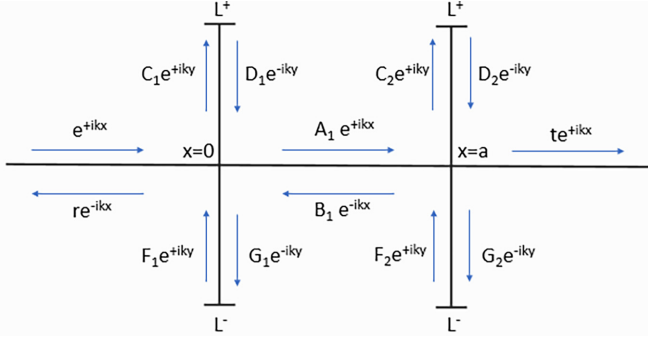
FIG. 12. System consisting of two identical crossbar junctions, separated by a distance a from one another.

$N = 2$ as

$$T = |t|^2 = \frac{1}{1 + |\alpha|^2 \left[\cos(ka) - \frac{[\cot(kL^+) + \cot(kL^-)]\sin(ka)}{2} \right]^2}. \tag{D1}$$

We seek to determine the local density of states for three regions of interest: the intermediate region between both junctions, the vertical region of the left crossbar, and the vertical region of the right crossbar. For this purpose, we calculate the coefficients by applying the corresponding boundary conditions shown in Eqs. (C5) to (C8) for $j = 1, 2$, $A_0 = 1$, $B_0 = r$, $A_1 = A$, $B_1 = B$, $A_2 = t$, and $B_2 = 0$. The results for the coefficients are

$$A = \frac{t(2 - \alpha)}{2}, \tag{D2}$$

$$B = \frac{t\alpha e^{2ika}}{2}, \tag{D3}$$

$$C_1 = \frac{t(2 - \alpha + \alpha e^{2ika})}{2(1 - e^{2ikL^+})}, \tag{D4}$$

$$D_1 = \frac{-t e^{2ikL^+}(2 - \alpha + \alpha e^{2ika})}{2(1 - e^{2ikL^+})}, \tag{D5}$$

$$G_1 = \frac{t(2 - \alpha + \alpha e^{2ika})}{2(1 - e^{2ikL^-})}, \tag{D6}$$

$$F_1 = \frac{-t e^{2ikL^-}(2 - \alpha + \alpha e^{2ika})}{2(1 - e^{2ikL^-})}, \tag{D7}$$

$$C_2 = \frac{t e^{ika}}{1 - e^{2ikL^+}}, \tag{D8}$$

$$D_2 = \frac{-t e^{2ikL^+} e^{ika}}{1 - e^{2ikL^+}}, \tag{D9}$$

$$G_2 = \frac{t e^{ika}}{1 - e^{2ikL^-}}, \tag{D10}$$

$$D_2 = \frac{-t e^{2ikL^-} e^{ika}}{1 - e^{2ikL^-}}. \tag{D11}$$

The local density of states for the region between junctions is calculated as

$$
\begin{aligned}
D_m &= \int_{x=0}^{x=a} |\Psi_m|^2 dx \\
&= \int_{x=0}^{x=a} [AA^* + BB^* + AB^* e^{2ikx} + A^* B e^{-2ikx}] dx \\
&= \int_{x=0}^{x=a} \left[\frac{2 + |\alpha|^2}{2} + \frac{-|\alpha|^2 - 2\alpha}{4} e^{2ik(x-a)} \right. \\
&\quad \left. + \frac{-|\alpha|^2 + 2\alpha}{4} e^{-2ik(x-a)} \right] |t|^2 dx. \tag{D12}
\end{aligned}
$$

For the vertical region of the left crossbar, we have

$$
\begin{aligned}
D_1 &= \int_{y=-L^-}^{y=L^+} |\Psi_1|^2 dy \\
&= \int_{y=0}^{y=L^+} \left| \Psi_1^A \right|^2 dy + \int_{y=-L^-}^{y=0} \left| \Psi_1^B \right|^2 dy, \tag{D13}
\end{aligned}
$$

with Ψ_1^A and Ψ_1^B being the wave functions for the upper and lower arms, respectively, and their quadratic values being

$$
\begin{aligned}
\left| \Psi_1^A \right|^2 &= [C_1 C_1^* + D_1 D_1^* + C_1 D_1^* e^{2iky} + C_1^* D_1 e^{-2iky}] \\
&= \frac{|t|^2 \{2 - 2\cos[2k(y - L^+)]\}}{2[2 - 2\cos(2kL^+)]} \\
&\quad \times \{2 - 2|\alpha|\sin(2ka) + |\alpha|^2[1 - \cos(2ka)]\}, \tag{D14} \\
\left| \Psi_1^B \right|^2 &= [F_1 F_1^* + G_1 G_1^* + F_1 G_1^* e^{2iky} + F_1^* G_1 e^{-2iky}] \\
&= \frac{|t|^2 \{2 - 2\cos[2k(y - L^-)]\}}{2[2 - 2\cos(2kL^-)]} \\
&\quad \times \{2 - 2|\alpha|\sin(2ka) + |\alpha|^2[1 - \cos(2ka)]\}. \tag{D15}
\end{aligned}
$$

And for the vertical region of the right crossbar, we have

$$
\begin{aligned}
D_2 &= \int_{y=-L^-}^{y=L^+} \left| \Psi_2 \right|^2 dy \\
&= \int_{y=0}^{y=L^+} \left| \Psi_2^A \right|^2 dy + \int_{y=-L^-}^{y=0} \left| \Psi_2^B \right|^2 dy, \tag{D16}
\end{aligned}
$$

with Ψ_2^A and Ψ_2^B being the wave functions for the upper and lower arms, respectively, and their quadratic values being

$$
\begin{aligned}
\left| \Psi_2^A \right|^2 &= [C_2 C_2^* + D_2 D_2^* + C_2 D_2^* e^{2iky} + C_2^* D_2 e^{-2iky}] \\
&= \frac{|t|^2 \{1 - \cos[2k(y - L^+)]\}}{1 - \cos(2kL^+)}, \tag{D17} \\
\left| \Psi_1^B \right|^2 &= [F_2 F_2^* + G_2 G_2^* + F_2 G_2^* e^{2iky} + F_2^* G_2 e^{-2iky}] \\
&= \frac{|t|^2 \{1 - \cos[2k(y - L^-)]\}}{1 - \cos(2kL^-)}. \tag{D18}
\end{aligned}
$$

[1] C. W. Hsu, B. Zhen, A. D. Stone, J. D. Joannopoulos, and M. Soljačić, Nat. Rev. Mater. **1**, 16048 (2016).

[2] A. F. Sadreev, Rep. Prog. Phys. **84**, 055901 (2021).

[3] J. von Neumann and E. Wigner, Phys. Z. **30**, 465 (1929) (in German).

[4] K. Koshelev, A. Bogdanov, and Y. Kivshar, Opt. Photon. News **31**, 38 (2020).

[5] H. Friedrich and D. Wintgen, Phys. Rev. A **32**, 3231 (1985).

[6] E. N. Bulgakov, K. N. Pichugin, A. F. Sadreev, and I. Rotter, JETP Lett. **84**, 430 (2006).

[7] N. Moiseyev, Phys. Rev. Lett. **102**, 167404 (2009).

[8] V. Fernández-Hurtado, J. Mur-Petit, J. J. García-Ripoll, and R. A. Molina, New J. Phys. **16**, 035005 (2014).

[9] J. Mur-Petit and R. A. Molina, Phys. Rev. B **90**, 035434 (2014).

[10] J. Mur-Petit and R. A. Molina, Phys. Rev. B **101**, 184306 (2020).

[11] M. L. Ladrón de Guevara, F. Claro, and P. A. Orellana, Phys. Rev. B **67**, 195335 (2003).

[12] M. L. Ladrón de Guevara and P. A. Orellana, Phys. Rev. B **73**, 205303 (2006).

[13] K. Koshelev, S. Lepeshov, M. Liu, A. Bogdanov, and Y. Kivshar, Phys. Rev. Lett. **121**, 193903 (2018).

[14] F. Capasso, C. Sirtori, J. Faist, D. L. Sivco, S.-N. G. Chu, and A. Y. Cho, Nature (London) **358**, 565 (1992).

[15] D. C. Marinica, A. G. Borisov, and S. V. Shabanov, Phys. Rev. Lett. **100**, 183902 (2008).

[16] T. Shi, Z. L. Deng, G. Geng, X. Zeng, Y. Zeng, G. Hu, A. Overvig, J. Li, C.-W. Qiu, A. Alù, Y. S. Kivshar, and X. Li, Nat. Commun. **13**, 4111 (2022).

[17] Y. Plotnik, O. Peleg, F. Dreisow, M. Heinrich, S. Nolte, A. Szameit, and M. Segev, Phys. Rev. Lett. **107**, 183901 (2011).

[18] R. A. Vicencio, C. Cantillano, L. Morales-Inostroza, B. Real, C. Mejía-Cortés, S. Weimann, A. Szameit, and M. I. Molina, Phys. Rev. Lett. **114**, 245503 (2015).

[19] L. Huang, Y. K. Chiang, S. Huang, C. Shen, F. Deng, Y. Cheng, B. Jia, Y. Li, D. A. Powell, and A. E. Miroshnichenko, Nat. Commun. **12**, 1 (2021).

[20] C. W. Hsu, B. Zhen, J. Lee, S.-L. Chua, S. G. Johnson, J. D. Joannopoulos, and M. Soljačić, Nature (London) **499**, 188 (2013).

[21] J. Jin, X. Yin, L. Ni, M. Soljačić, B. Zhen, and C. Peng, Nature (London) **574**, 501 (2019).

[22] D. R. Abujetas, J. J. Sáenz, and J. A. Sánchez-Gil, J. Appl. Phys. **125**, 183103 (2019).

[23] I. Quotane, M. Amrani, C. Ghouila-Houri, E. H. El Boudouti, L. Krutyansky, B. Piwakowski, P. Pernod, A. Talbi, and B. Djafari-Rouhani, Crystals **12**, 707 (2022).

[24] R. E. Jacobsen, A. Krasnok, S. Arslanagić, A. V. Lavrinenko, and A. Alú, ACS Photon. **9**, 1936 (2022).

[25] A. Kodigala, T. Lepetit, Q. Gu, B. Bahari, Y. Fainman, and B. Kanté, Nature (London) **541**, 196 (2017).

[26] S. T. Ha, Y. H. Fu, N. K. Emani, Z. Pan, R. M. Bakker, R. Paniagua-Domínguez, and A. I. Kuznetsov, Nat. Nanotechnol. **13**, 1042 (2018).

[27] J. M. Foley, S. M. Young, and J. D. Phillips, Phys. Rev. B **89**, 165111 (2014).

[28] Z. Yu and X. Sun, Light: Sci. Appl. **9**, 1 (2020).

[29] H. Qin, W. Redjem, and B. Kante, Opt. Lett. **47**, 1774 (2022).

[30] P. K. G Berkolaiko, *Introduction to Quantum Graphs* (American Mathematical Society, Providence, RI, 2013).

[31] K.-K. Voo and C. S. Chu, Phys. Rev. B **74**, 155306 (2006).

[32] T. Lawrie, S. Gnutzmann, and G. Tanner, J. Phys. A **56**, 475202 (2023).

[33] L. Dobrzyński, H. Al-Wahsh, A. Akjouj, and E. A. Abdel-Ghaffar, Phys. Rev. B **108**, 115426 (2023).

[34] N. Cortés, L. Chico, M. Pacheco, L. Rosales, and P. A. Orellana, Europhys. Lett. **108**, 46008 (2014).

[35] L. Xu, K. Z. Kamali, L. Huang, M. Rahmani, A. Smirnov, R. Camacho-Morales, Y. Ma, G. Zhang, M. Woolley, D. Neshev, and A. E. Miroshnichenko, Adv. Sci. **6**, 1802119 (2019).

[36] Z. Liu, Y. Xu, Y. Lin, J. Xiang, T. Feng, Q. Cao, J. Li, S. Lan, and J. Liu, Phys. Rev. Lett. **123**, 253901 (2019).

[37] M. Born and E. Wolf, *Principles of Optics: Electromagnetic Theory of Propagation, Interference and Diffraction of Light*, 2nd ed. (Pergamon, Oxford, 1964).

[38] M. F. Limonov, Adv. Opt. Photon. **13**, 703 (2021).

[39] P. Markos and C. M. Soukoulis, in *Wave Propagation* (Princeton University Press, Princeton, NJ, 2008), p. 4.

[40] W. Maimaiti, A. Andreanov, H. C. Park, O. Gendelman, and S. Flach, Phys. Rev. B **95**, 115135 (2017).

[41] S. V. Nabol, P. S. Pankin, D. N. Maksimov, and I. V. Timofeev, Phys. Rev. B **106**, 245403 (2022).

[42] S. Khattou, Y. Rezzouk, M. El Ghafiani, M. Amrani, M. Elaouni, E. H. El Boudouti, A. Talbi, A. Akjouj, and B. Djafari-Rouhani, Phys. Rev. B **107**, 125405 (2023).

[43] G. Siroki, P. A. Huidobro, and V. Giannini, Phys. Rev. B **96**, 041408(R) (2017).

[44] D. J. Griffiths and D. F. Schroeter, *Introduction to Quantum Mechanics* (Cambridge University Press, Cambridge, 2018).